


Article

Hydrogen Production via the Oxy-Steam Reforming of LNG or Methane on Ni Catalysts

Paweł Mierczynski * , Natalia Stepieńska, Magdalena Mosinska, Karolina Chalupka, Jadwiga Albinska, Waldemar Maniukiewicz , Jacek Rogowski, Magdalena Nowosielska and Malgorzata I. Szyrkowska * 

Institute of General and Ecological Chemistry, Lodz University of Technology, Zeromskiego 116, 90-924 Lodz, Poland; natalia.stepinska1996@gmail.com (N.S.); magdalena.mosinska@dokt.p.lodz.pl (M.M.); karolina.chalupka@p.lodz.pl (K.C.); jadwiga.albinska@p.lodz.pl (J.A.); waldemar.maniukiewicz@p.lodz.pl (W.M.); jacek.rogowski@p.lodz.pl (J.R.); magdalena.nowosielska@p.lodz.pl (M.N.)

* Correspondence: pawel.mierczynski@p.lodz.pl (P.M.); malgorzata.szyrkowska@p.lodz.pl (M.I.S.); Tel.: +48-42-631-31-25 (P.M.); +48-42-631-30-99 (M.I.S.)

Received: 25 February 2020; Accepted: 17 March 2020; Published: 20 March 2020



Abstract: Ni catalysts supported on ZrO_2 , 5% CeO_2 - ZrO_2 , and 5% La_2O_3 - ZrO_2 were prepared via the impregnation method and tested in the oxy-steam reforming of methane and liquified natural gas (LNG). All tested catalysts exhibited high catalytic activity in the studied process at 700 and 900 °C. The improvement of the stability of Ni catalysts after the addition of CeO_2 oxide in the studied oxy-steam reforming of LNG process was confirmed. In addition, high activity and selectivity towards hydrogen was proven in the oxy-steam reforming process at 900 °C over a 20%Ni/5% CeO_2 - ZrO_2 catalyst. It was also proved that the addition of CeO_2 onto a ZrO_2 carrier leads to a decrease in the NiO and metallic Ni crystallite sizes that were detected by the X-Ray diffraction (XRD) technique. The solid solution formation between NiO and ZrO_2 and/or NiO and CeO_2 was proved. Superior reactivity in the oxy-steam reforming of CH_4 and the LNG process exhibited a 20%Ni/ ZrO_2 catalyst, which showed the highest methane conversions at 500 and 600 °C, equal to 63% and 89%, respectively. In addition, also in the case of the LNG reforming reaction, the most active catalyst was the 20%Ni/ ZrO_2 system, which demonstrated 46.3% and 76.9% of the methane conversion value at 500 and 600 °C and the total conversion of others hydrocarbons (ethane, propane and butane). In addition, this catalytic system exhibited the highest selectivity towards hydrogen formation in the oxy-steam reforming of the LNG reaction equal to 71.2% and 71.3% at 500 and 600 °C, respectively. The highest activity of this system can be explained by the uniform distributions of Ni species and their highest concentration compared to the rest of the monometallic Ni catalysts. Time-of-flight secondary ion mass spectrometry (ToF-SIMS) results also confirmed a strong interaction of NiO with ZrO_2 in the case of the 20%Ni/ ZrO_2 catalysts. The presence of selected NiZrO^+ ions emitted from the investigated surface of the 20%Ni/ ZrO_2 system was detected.

Keywords: reforming of methane; LNG; nickel catalysts; syngas; ZrO_2 ; reforming of liquid natural gas

1. Introduction

The development of civilization, the progressive degradation of the environment, and the growing scarcity of raw materials, especially energetic, caused an increased interest in alternative energy sources and the modern technologies involved in their production. Accordingly, studies of many research and development centers are focused not only on issues related to the production, transport, storage, and use of hydrogen energy, but also are related to the search for new methods of producing high

purity hydrogen, which is directly related to the use of fuel cell technology [1–5]. Currently, the main technologies of the hydrogen production are based on the steam reforming of natural gas. The hydrogen production via the reforming process of natural gas consists of two stages. The first step is connected with the purification of natural gas from the sulphur and nitrogen compounds. The second step involves the proper steam reforming of methane and higher hydrocarbons. A two-stage process makes it impossible to obtain hydrogen in one reaction act. The solution of this problem is liquefied natural gas (LNG) [6,7]. The main component of LNG is methane, whose content ranges from 88.4% to 99.7% and its other components include ethane (0.1–13.4%), propane (0–3.7%), C₄ (0–1.5%), and nitrogen (0–0.8%). After the condensation of the natural gas, a very pure, colourless, and odourless gas mixture mainly consisting of hydrocarbons is obtained without toxic and corrosive properties [8]. Therefore, hydrogen production via the steam reforming of liquefied natural gas (LNG) can be a promising route due to well-established LNG supply infrastructures and wide-spreading LNG pipelines in the modern cities [6].

A typical catalyst used in the reforming of natural gas was Ni/Al₂O₃-based catalysts [9–11]. Many scientists have investigated the influence of the different promoters on the catalytic activity, stability, and selectivity of Ni catalysts in reforming processes. Some authors reported an improvement in the Ni catalysts stability after CeO₂ addition into an Ni system. In addition, some evidence that cerium oxide stabilizes Al₂O₃ support and provides the mobile oxygen during oxidation and reduction conditions can also be found [12–14]. It is also known that cerium oxide addition improves the catalytic activity and protects against a carbon build-up of Ni-based catalysts [13]. On the other hand, the addition of La₂O₃ oxide into an Ni-based system, increasing the NiO dispersion on the support surface, facilitates the reduction of the NiO phase. This modifier facilitates the oxidation of carbon forms created on the catalyst surface and limits the carbon deposit formation during the reforming of the methane process, which leads to increasing the Ni catalyst's stability [15,16].

Therefore, the main aim of this work was to determine the effect of Ni and the influence of the modifiers on the physicochemical and catalytic properties of nickel catalysts in the oxy-steam reforming of methane or LNG reaction. In order to achieve the intended purposes of the presented work, monometallic nickel catalysts supported on ZrO₂, 5%CeO₂-ZrO₂, 5%La₂O₃-ZrO₂ with different loadings (5, 10, 20, 30% wt.) of Ni were prepared by the impregnation method. Their physicochemical properties were extensively studied by Brunauer–Emmett–Teller (BET), Temperature-Programmed-Reduction in hydrogen (TPR-H₂), Temperature-Programmed-Desorption of ammonia (TPD-NH₃), XRD, Scanning Electron Microscope with EDS detector (SEM-EDS), and Thermal Analysis coupled with Mass Spectrometer (TG-DTA-MS) techniques. In order to correlate the catalytic activity of the catalysts with their physicochemical properties in the oxy-steam reforming of methane or LNG catalytic activity, measurements were done using a fixed bed micro-reactor under atmospheric pressure in the temperature range 500–900 °C.

2. Results and Discussion

2.1. Activity Tests

Catalytic tests in the oxy-steam reforming of methane were performed in the fixed bed microreactor under atmospheric pressure in the temperature range 500–900 °C. In the first step of the activity measurements, the influence of Ni loading on the catalytic activity of monometallic systems (Ni/ZrO₂) in the oxy-steam reforming of methane reaction was studied. The activity measurements were expressed as methane conversions, selectivity towards CO and CO₂, and hydrogen yield. The results obtained for Ni catalysts containing 5, 10, 20 and 30% wt. of Ni are given in Figure 1. The activity results show that the highest methane conversion at 700 °C, the yield of the hydrogen formation, and the highest molar ratio between H₂ and CO was obtained (H₂/CO = 2.0 at 700 °C) for 30%Ni/ZrO₂ catalyst. At 900 °C, the highest hydrogen yield was obtained using the 20%Ni/ZrO₂ catalyst. From the application point of view, for the next catalytic tests, we selected a system containing 20% wt. of Ni due to the lower content of nickel in the catalytic system and the fact that this system is characterized

by high methane conversion and efficiency in the production of hydrogen. Next, the influence of structural additives such as CeO_2 or La_2O_3 on the catalytic and physicochemical properties of the 20%Ni/ZrO₂ catalyst was also studied in this work and the results are shown in Figure 2. The activity tests performed for the catalysts containing 20% wt. of Ni showed that the reaction runs from 500 °C. At this temperature, the highest activity was obtained using the 20%Ni/ZrO₂ system, which exhibited 7.4% of methane conversion compared to the nickel catalysts with CeO_2 and La_2O_3 addition. At 600 °C the highest methane conversion of 13.9% was observed for catalysts with 5% La_2O_3 addition. Meanwhile, further increasing the reaction temperature up to 700 °C showed that the 20%Ni/ZrO₂ and 20%Ni/5% La_2O_3 -ZrO₂ catalysts exhibited practically the same methane conversion above 97%. Whereas, the 20%Ni/5% CeO_2 -ZrO₂ system showed the CH₄ conversion was equal to 86.7% together with the highest hydrogen yield (70.7%). It should be also noted that all Ni catalysts with 20% of nickel loading showed total conversion of methane at 900 °C.

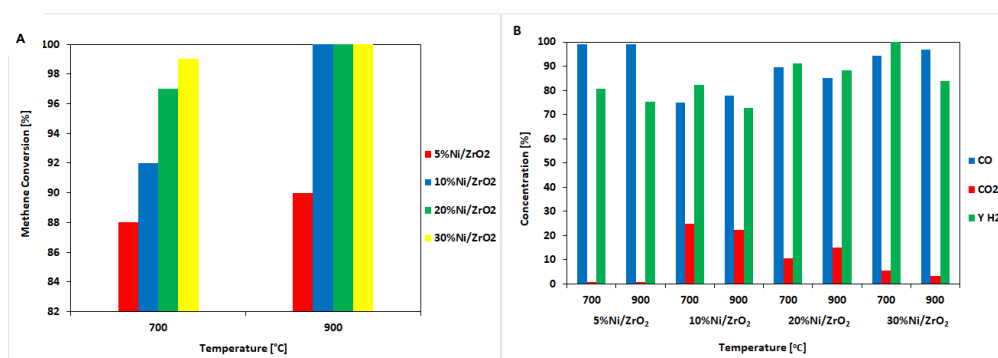


Figure 1. Catalytic activity results obtained for monometallic Ni/ZrO₂ catalysts in the oxy-steam reforming of methane expressed as methane conversion, and the selectivity of the CO and CO₂ and hydrogen yield formed during the process. (A) Methane conversion. (B) The selectivity towards CO and CO₂ and hydrogen yield.

Furthermore, the 20%Ni/ZrO₂ catalyst exhibited the highest hydrogen formation (64.6%), and the highest H₂/CO molar ratio was equal to 2.2 during the investigated process. It should be also emphasized that this catalyst exhibited the highest selectivity towards hydrogen generation at 700 and 900 °C among of all investigated catalysts containing 20% wt. of Ni.

In the next step of the catalytic activity measurements, the oxy-steam reforming of LNG was investigated. The oxy-steam reforming of LNG was investigated over a series of the catalysts containing 20%wt. of Ni, and the catalytic measurements are shown in Figures 3–5. The results of the activity measurements showed that, starting from 400 °C, we observed the conversion of methane, ethane, propane, and butane equal to 18.8%, 24.7%, 36.8%, and 100% in the oxy-steam reforming of LNG over 20%Ni/ZrO₂ catalyst, respectively (see Figure 3). On the other hand, the activity results show that when the reaction is carried out at 400 °C using a 20%Ni/5% La_2O_3 -ZrO₂ catalyst, only a low conversion of propane and butane was detected (see Figure 4). While, 20%Ni/5% CeO_2 -ZrO₂ catalysts also exhibited lower conversion values compared to the not-promoted Ni catalyst (43.7% of butane, 22.2% of propane, 11.9% of ethane, and 4.6% of methane, see Figure 5). Increasing the reaction temperature up to 500 °C results in 100% of ethane, propane and butane conversions during the reaction performed on 20%Ni/ZrO₂ catalysts. Whereas, the catalytic activity results obtained for the promoted catalysts confirmed the incomplete conversion of methane, ethane, and propane. Further raising the reaction temperature up to 600 °C resulted in the full conversion of the higher hydrocarbons (ethane, propane, butane) for the 20%Ni/ZrO₂ and 20%Ni/5% CeO_2 -ZrO₂ systems. However, in the case of the 20%Ni/5% La_2O_3 -ZrO₂ system, we also detected an incomplete conversion of ethane and propane. At 600 °C, the highest hydrogen yield formation had 20%Ni/ZrO₂ catalyst (74%). The results obtained at 700 and 900 °C gave evidence that in all cases we observed the total conversion of the higher hydrocarbons (ethane, propane, and butane) and that the methane conversion was above 94%. It is

also worth mentioning that the promoted Ni catalysts (20%Ni/5%La₂O₃-ZrO₂, 20%Ni/5%CeO₂-ZrO₂) showed higher hydrogen yield together with a high molar ratio between the created products of H₂/CO at 700 °C compared to the 20%Ni/ZrO₂ catalyst.

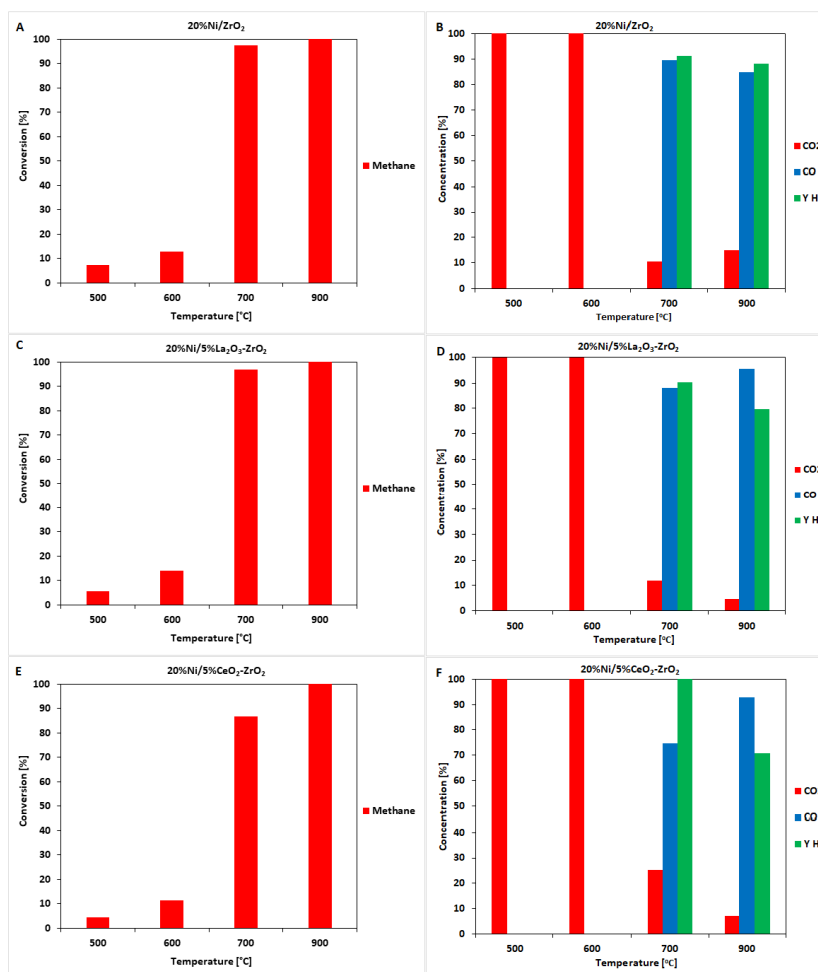


Figure 2. Catalytic activity results obtained in the oxy-steam reforming of methane expressed as methane conversion, and the selectivity of the CO and CO₂ formed during the process and hydrogen yield. (A,B)—20%Ni/ZrO₂, (C,D)—20%Ni/5%La₂O₃-ZrO₂, (E,F)—20%Ni/5%CeO₂-ZrO₂.

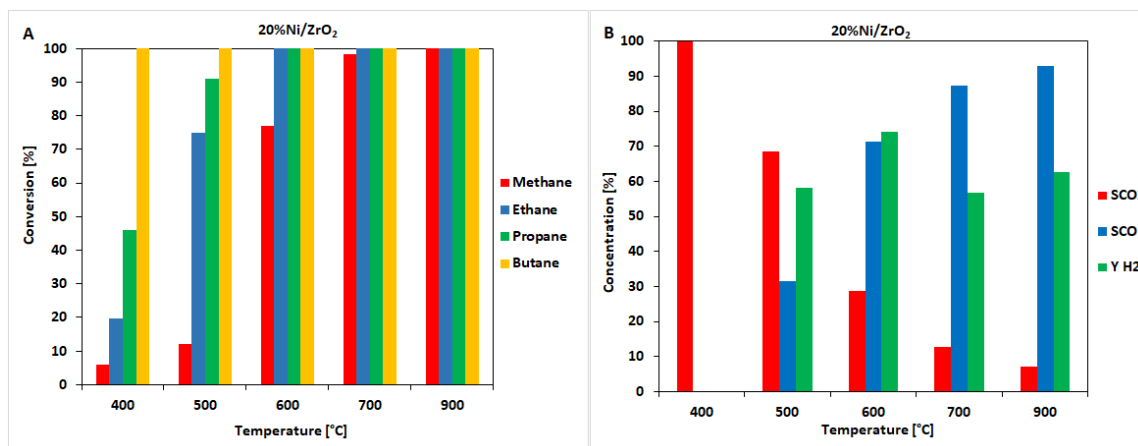


Figure 3. Results of the catalytic activity measurements performed in the temperature range 400–900 °C in the OSRM of a liquified natural gas (LNG) reaction on a 20%Ni/ZrO₂ catalyst. (A) Hydrocarbon conversion. (B) The selectivity of CO and CO₂ and hydrogen yield.

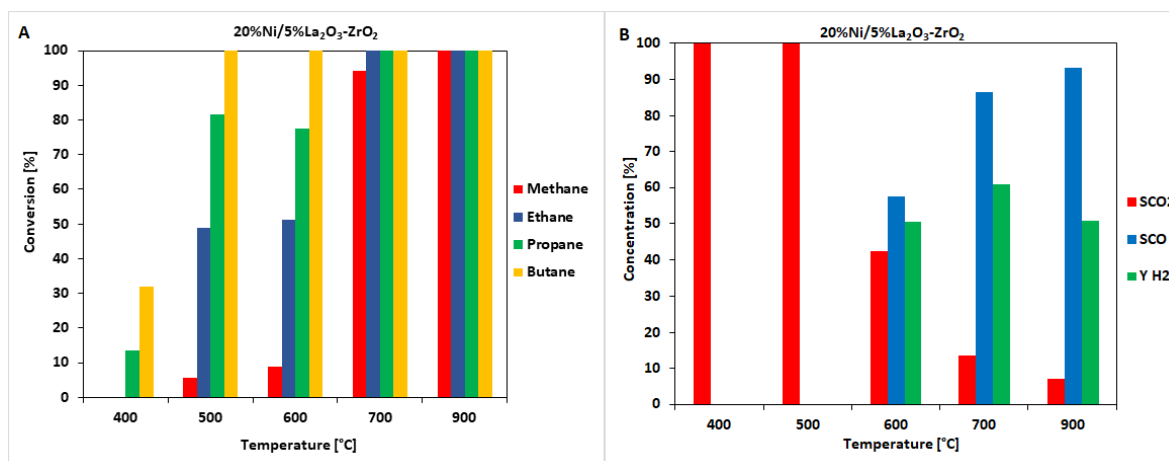


Figure 4. Results of the catalytic activity measurements performed in the temperature range 400–900 °C in the OSRM of the LNG reaction on a 20%Ni/5%La₂O₃-ZrO₂ catalyst. (A) Hydrocarbon conversion. (B) The selectivity of CO and CO₂ and hydrogen yield.

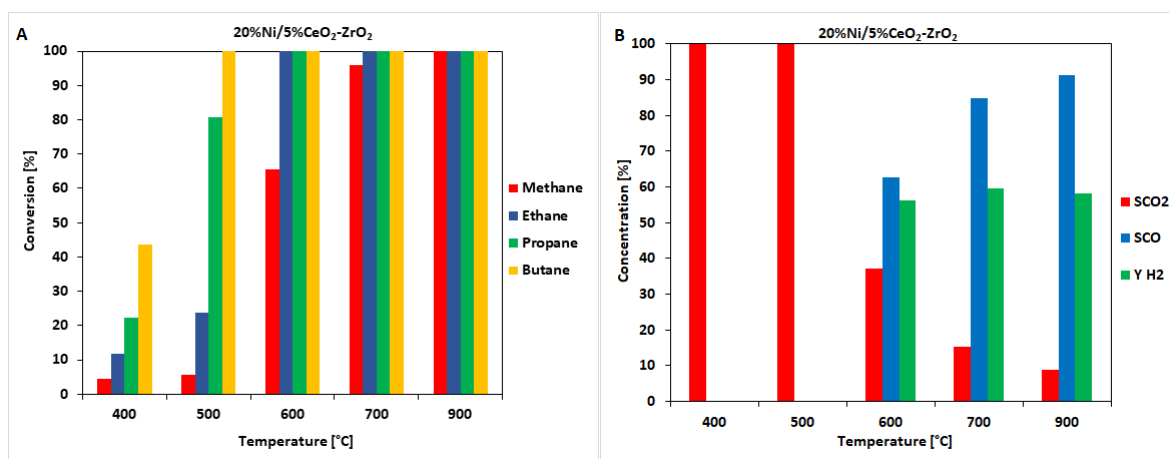


Figure 5. Results of the catalytic activity measurements performed in the temperature range 400–900 °C in the OSRM of the LNG reaction on a 20%Ni/5%CeO₂-ZrO₂ catalyst. (A) Hydrocarbon conversion. (B) The selectivity of CO and CO₂ and hydrogen yield.

On the other hand, the 20%Ni/5%CeO₂-ZrO₂ and 20%Ni/5%La₂O₃-ZrO₂ catalysts exhibited a higher H₂/CO molar ratio in the outlet gases during the reaction performed at 700 and 900 °C. Summarizing the catalytic activity of the Ni catalysts performed in the oxy-steam reforming of LNG, it should be emphasized that above 600 °C the reaction runs in the same way as in the case of the oxy-steam reforming of the methane process. The main products observed in the outlet gases are CO₂, H₂, and CO. It should be also noticed that at 600 °C we obtained very satisfactory results for the 20%Ni/ZrO₂ and 20%Ni/5%CeO₂-ZrO₂ catalyst. These systems showed a high conversion of methane, above 65%, and a high yield of hydrogen generation equal to 74% and 56% for the 20%Ni/ZrO₂ and 20%Ni/5%CeO₂-ZrO₂ catalysts, respectively. It should be also noticed that both the 20%Ni/5%CeO₂-ZrO₂ and 20%Ni/5%La₂O₃-ZrO₂ catalysts exhibited high hydrocarbon conversions and the higher hydrogen yield at 700 °C compared to the 20%Ni/ZrO₂ system. While, at 900 °C, the highest hydrogen yield was obtained using 20%Ni/ZrO₂, which exhibited a total conversion of methane and other hydrocarbons. These results confirm the possibility of using LNG for hydrogen production to power fuel cells.

Next, the catalytic tests during the 12 h of the reaction for the 20%Ni/ZrO₂, 20%Ni/5%La₂O₃-ZrO₂ and 20%Ni/5%CeO₂-ZrO₂ were carried out in the oxy-steam LNG reforming process at 700 °C, and the results are given in Figures 6–8, respectively. The results of the time-on-stream catalytic tests

showed that all investigated catalysts were stable during the process. It should be emphasized that the Ni catalyst with La_2O_3 addition exhibited stable methane conversion equal to 99% and other light hydrocarbon conversions (ethane, propane, butane) after 4h of the running the process. Other tested catalysts showed slight changes in methane conversion values during the period of catalytic tests. In addition, all three catalysts showed very similar selectivity towards CO and CO_2 and hydrogen yield.

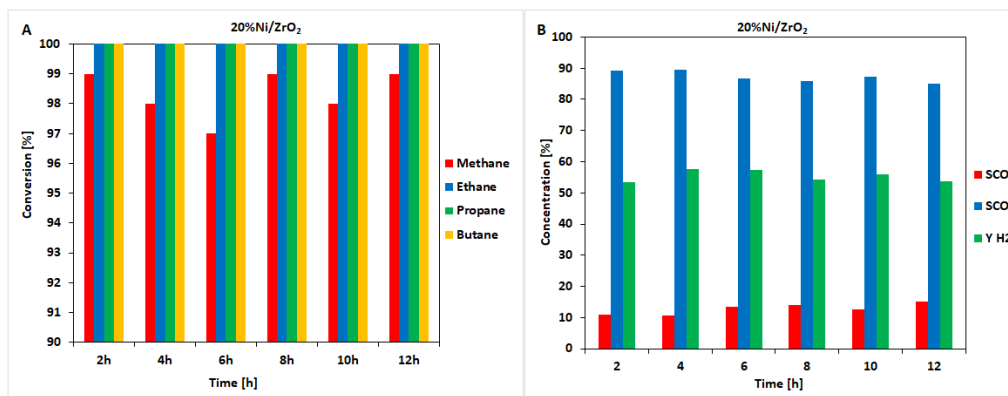


Figure 6. Results of the time-on-stream catalytic tests performed during 12 h of the OSRM of the LNG reaction on a 20%Ni/ZrO₂ catalyst. (A) Hydrocarbon conversion. (B) The selectivity of CO and CO₂ and hydrogen yield.

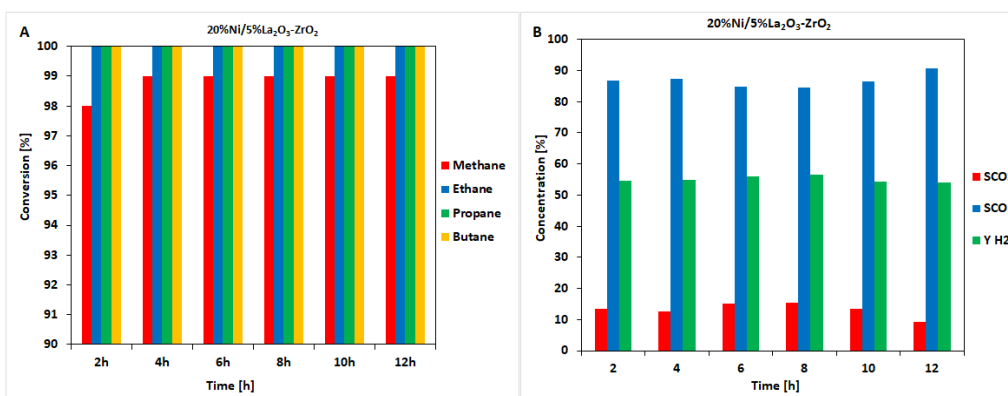


Figure 7. Results of the time-on-stream catalytic tests performed during 12 h of the OSRM of the LNG reaction on a 20%Ni/5%La₂O₃-ZrO₂ catalyst. (A) Hydrocarbon conversion. (B) The selectivity of the CO and CO₂ and hydrogen yield.

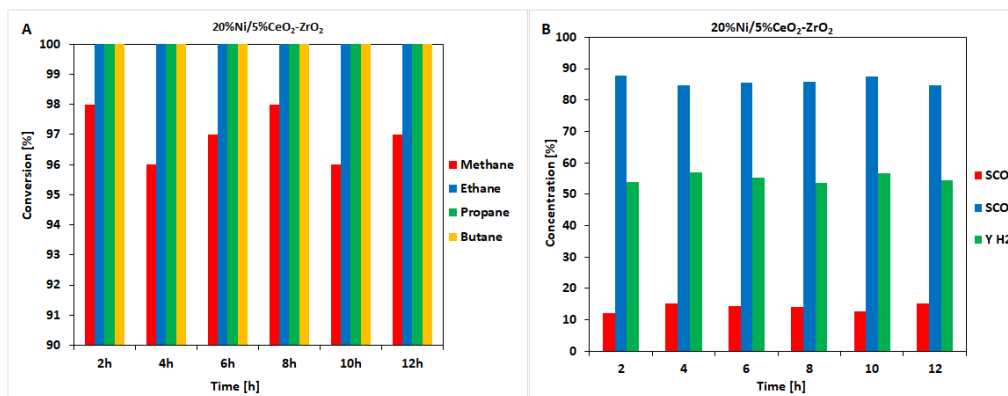


Figure 8. Results of the time-on-stream catalytic tests performed during 12 h of the OSRM of the LNG reaction on a 20%Ni/5%CeO₂-ZrO₂ catalyst. (A) Hydrocarbon conversion. (B) The selectivity of the CO and CO₂ and hydrogen yield.

2.2. Phase Composition Studies of the Catalytic Material

In order to correlate the reactivity of the Ni catalysts with the properties in the oxy-steam reforming of the LNG process, their physicochemical properties were investigated using various research techniques. The phase composition studies of the supports and Ni-calcined catalysts were studied using a conventional XRD technique, and the results are shown in Figures 9 and 10. The phase composition studies of ZrO_2 showed that this support consists of the tetragonal and monoclinic structure of the ZrO_2 phase [17]. The XRD measurements performed for the calcined Ni systems confirmed the presence of the NiO, tetragonal, and monoclinic crystallographic structure of ZrO_2 phases on the diffraction patterns [11] (see Figure 9). The addition of La_2O_3 or CeO_2 oxide into the ZrO_2 structure did not cause any changes in the phase composition of the investigated catalytic material (see Figure 10). The diffraction curves recorded for the 20%Ni/5% CeO_2 - ZrO_2 and 20%Ni/5% La_2O_3 - ZrO_2 catalysts showed the presence of the same crystallographic phases that were detected for the Ni/ ZrO_2 catalyst. The only differences were observed for the 20%Ni/5% CeO_2 - ZrO_2 catalyst. On the diffraction curve recorded for this system, the shift of the diffraction peaks assigned to the ZrO_2 phases towards the lower 2 theta angle was observed compared to 20%Ni/ ZrO_2 . These shifts of the diffraction peaks of zirconia may be explained by the presence of a solid solution between CeO_2 and ZrO_2 created during the preparation of the catalytic material.

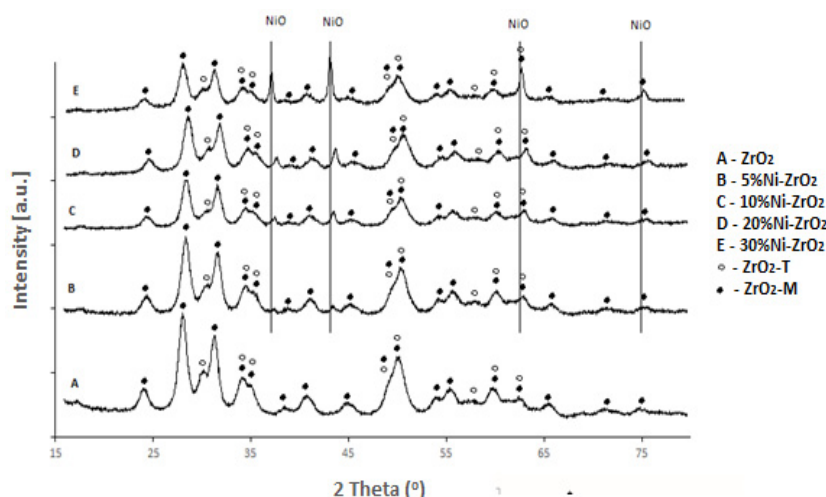


Figure 9. XRD curves of the ZrO_2 and monometallic Ni/ ZrO_2 catalysts calcined in an air atmosphere for 4h at 400 °C.

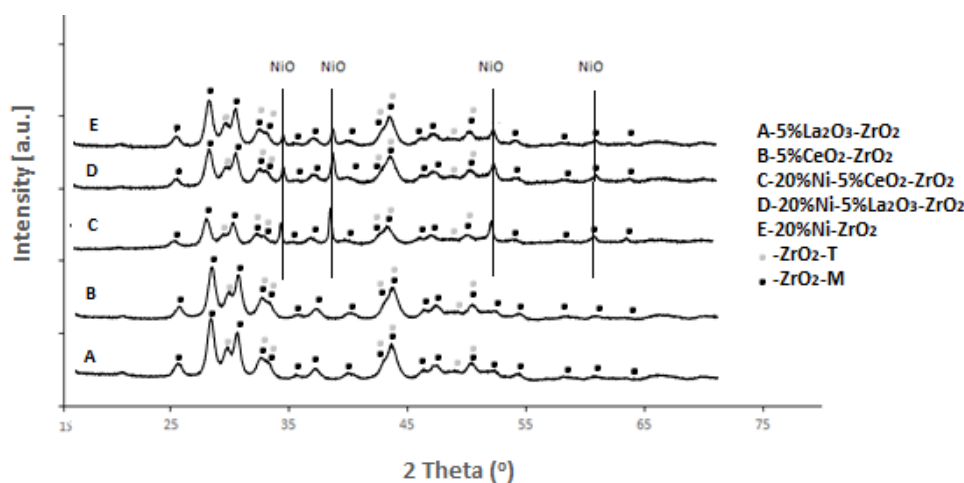


Figure 10. XRD curves of supports 5% La_2O_3 - ZrO_2 , 5% CeO_2 - ZrO_2 , and monometallic Ni catalysts supported on ZrO_2 , 5% CeO_2 - ZrO_2 , and 5% La_2O_3 - ZrO_2 calcined in an air atmosphere for 4h at 400 °C.

Furthermore, the phase composition studies of spent 20%Ni catalysts supported on ZrO_2 , 5% La_2O_3 - ZrO_2 , and 5% CeO_2 - ZrO_2 carriers were given in Figure 11. The results confirm the presence of monoclinic and tetragonal ZrO_2 and metallic nickel phases on the diffractions curves. It is also worth emphasizing that the catalytic systems and the average size of the nickel oxide and metallic nickel crystallites were calculated based on the Scherrer's formula which is presented below:

$$D = Kl/(\cos\theta)$$

where D is the averaged dimension of the crystallites, K is the Scherrer constant. In the formula represented above, K is the wavelength of X-ray ($\text{CuK}\alpha = 0.154 \text{ nm}$), and B is the width of the peak at half height. The results of the calculation performed for the calcined catalysts are given in Table 1. The obtained results show that the lowest crystallites size of NiO was observed for the 20%Ni-5% La_2O_3 - ZrO_2 system, while the largest size of the NiO crystallites was detected for the 20Ni% ZrO_2 catalyst (see Figure 10).

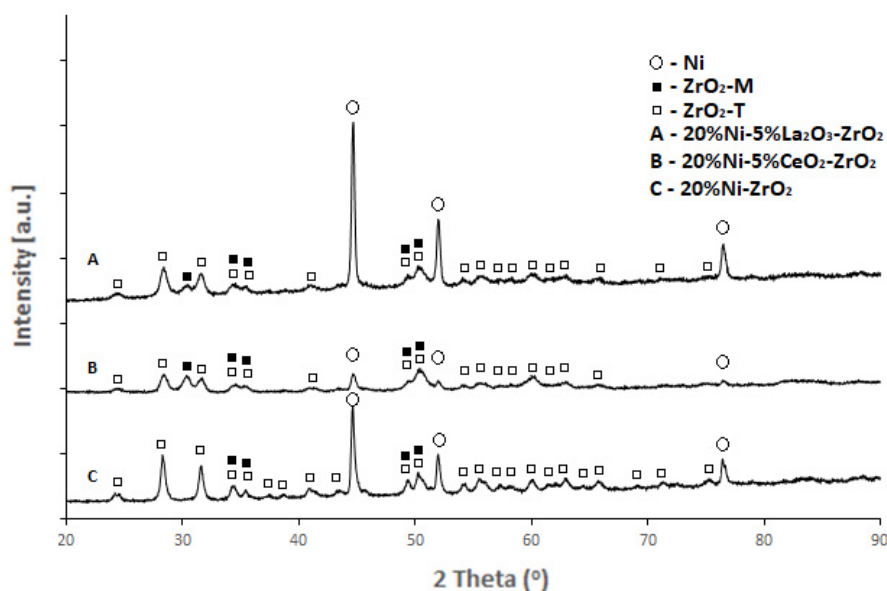


Figure 11. XRD curves of spent 20%Ni catalysts supported on ZrO_2 , 5% La_2O_3 - ZrO_2 , and 5% CeO_2 - ZrO_2 carriers.

Table 1. Size of NiO crystallites estimated by the Scherrer method for a NiO peak (200) for an angle of $2\theta = 43.36^\circ$ obtained from XRD measurements performed for Ni catalysts calcined in an air atmosphere at 400°C for 4 h.

No.	Catalyst	The Size of NiO Crystallites [nm]
1	20Ni% ZrO_2	32
2	20%Ni-5% CeO_2 - ZrO_2	24
3	20%Ni-5% La_2O_3 - ZrO_2	20

Afterwards, spent Ni catalysts were tested using the same XRD technique. The X-ray patterns recorded for the Ni systems containing 20 wt.% of Ni are shown in Figure 11. The obtaining results clearly show the diffraction peaks located at about 2θ angle 44.5° . The occurrence of these peaks proves the formation of the metallic nickel phase. The profiles fitting for the Ni (111) peaks were successful and gave average crystallite sizes of metallic Ni for all investigated catalytic systems, and the obtained results are presented in Table 2. As can be seen, the lowest crystallites of metallic Ni had the 20%Ni/5% CeO_2 - ZrO_2 catalyst. While the highest crystallites of Ni $^\circ$ particles owned spent the 20%Ni/5% La_2O_3 - ZrO_2 catalyst, which exhibited the lowest catalytic activity in the investigated

oxy-steam reforming process of LNG. Considering the obtained XRD results, it should be emphasized that only in the case of a catalyst with the addition of La_2O_3 is a significant increase in metallic nickel crystallites' size observed after the oxy-steam reforming of LNG.

Table 2. Crystallite size of metallic nickel calculated from XRD measurements performed for spent Ni catalysts (after catalytic tests performed in the oxy-steam reforming of LNG process in the temperature range 400–700 °C, a molar ratio between reagents was used: $\text{C:H}_2\text{O:O}_2 = 1:2.7:0.35$, the total gas flow was $51 \text{ cm}^3/\text{min}$).

No.	Catalyst	The Size of Ni ⁰ Crystallites [nm]
1	20%Ni/ZrO ₂	35
2	20%Ni/5%CeO ₂ -ZrO ₂	22
3	20%Ni/5%La ₂ O ₃ -ZrO ₂	41

2.3. Reducibility Studies of Catalytic Materials

The reducibility of the Ni catalysts was studied using TPR-H₂ method, and the results for ZrO₂ oxide and Ni catalysts supported on this carrier are given in Figure 12.

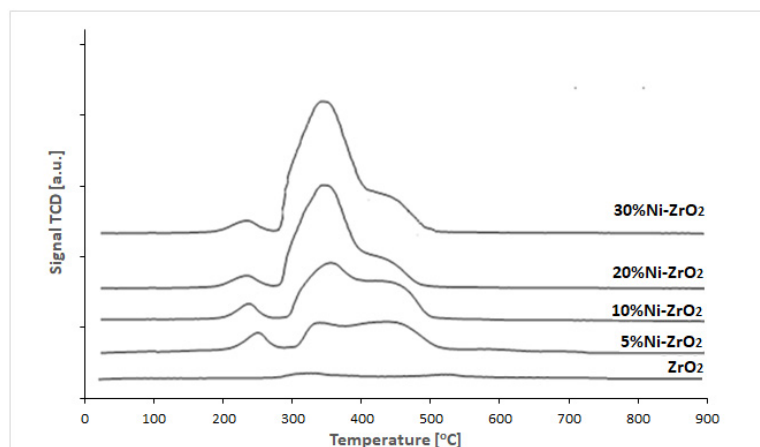


Figure 12. Temperature programmed reduction profiles of ZrO₂ and Ni catalysts supported on ZrO₂ oxide calcined in an air atmosphere for 4h at 400 °C.

TPR-H₂ profile recorded for the carrier itself shows two reduction stages located at about 310 and 520 °C assigned to the reversible hydrogen uptake of the ZrO₂ surface [18,19]. Temperature programmed reduction studies performed for Ni catalysts confirmed a three-stage reduction process of the Ni systems. The TPR-H₂ curve recorded for the 5%Ni/ZrO₂ catalyst showed three reduction stages. The first effect located at about 230 °C is assigned to the reduction of free NiO species located on the support surface. The next two reduction effects located at 320 and 440 °C are assigned to the reduction of NiO interacted with support [6]. Similar reduction behavior was observed in the work [20,21]. The increase of the Ni loading in the catalytic systems shifts the reduction stages towards a lower temperature range and an increase in the intensities assigned to the low temperature effects. In the next step, we investigated the influence of CeO₂ and La₂O₃ oxides addition on the reducibility of the 20%Ni catalysts. Figure 13 presents the reduction behavior of the 20%Ni catalysts supported on ZrO₂, 5%La₂O₃-ZrO₂, and 5%CeO₂-ZrO₂ carriers. The presented results clearly show that the addition of 5%La₂O₃ improves the NiO reduction that is manifested by the increase of the reduction peaks intensity compared to the reduction effects observed in the TPR-H₂ profile of the Ni/ZrO₂ catalyst. In addition, it should be also emphasized that the addition of La₂O₃ into the 20%Ni/ZrO₂ system caused the increase in the intensity of the reduction stage, with the maximum of the hydrogen consumption peak located at 340 °C.

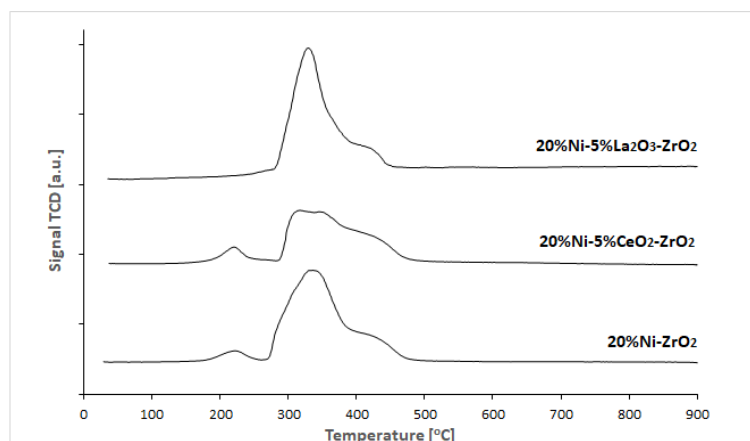


Figure 13. Temperature programmed reduction profiles of 20%Ni catalysts supported on 5%La₂O₃-ZrO₂, 5%CeO₂-ZrO₂, and ZrO₂ calcined in an air atmosphere for 4h at 400 °C.

The influence of the 5%CeO₂ addition on the reduction behavior of Ni/ZrO₂ catalyst is also presented in Figure 13. The reduction profile recorded for the 20%Ni/5%CeO₂-ZrO₂ system shows the same reduction stages that were observed in the case of the Ni/ZrO₂ system. In addition, the TPR-H₂ reduction profile of 20%Ni/5%CeO₂-ZrO₂ shows the slight shift of the reduction stages towards higher temperature compared to the Ni system supported on ZrO₂. This result confirms the stronger interaction between NiO species and support components [14], compared to the 20%Ni/ZrO₂ catalyst. A similar tendency was also observed by Takeguchi and co-workers [14].

In addition, the reduction degree of nickel catalysts was determined based on the hydrogen consumption peaks. An amount of hydrogen consumed during each TPR run was presented in Table 3. The results clearly show that increasing the Ni content from 10 to 20% wt. of Ni in the investigated catalyst leads to a decrease in the hydrogen consumption for Ni/ZrO₂ catalysts from 99% to 80% (see Table 3), while further increasing the Ni content in the catalytic material leads to the degree of reduction equal 71% estimated for the 30%Ni/ZrO₂ catalyst. In the case of the catalysts containing 20% wt. of Ni, the estimated reduction degree values show that the highest hydrogen consumption was achieved using the 20%Ni/5%La₂O₃-ZrO₂ (3.36×10^{-4} mol of H₂) catalyst. On the other hand, the lowest degree of the reduction value (60%) was achieved using the 20%Ni/5%CeO₂-ZrO₂ supported catalyst. The reduction of NiO on the catalysts with a high metal loading may be hindered in the case of the strong interaction between NiO and ZrO₂ or NiO and CeO₂. The incomplete reduction confirmed by the reduction degree calculated for the investigated catalysts can be explained by the strong interaction between NiO and the support component or by the solid solution formation between these species [3].

Table 3. Amount of hydrogen consumed during the TPR run and the estimated reduction degree for the nickel catalysts.

Catalysts	H ₂ Consumed (mol/g _{cat}) × 10 ⁺⁴	Reduction of NiO (%)
5%Ni/ZrO ₂	0.84	99
10%Ni/ZrO ₂	1.69	99
20%Ni/ZrO ₂	2.70	80
30%Ni/ZrO ₂	3.60	71
20%Ni/5%La ₂ O ₃ -ZrO ₂	3.36	99
20%Ni/5%CeO ₂ -ZrO ₂	2.01	60

2.4. Specific Surface Area Measurements of Supports and Monometallic Nickel Catalysts

The specific surface area (SSA) measurements performed for ZrO₂ and monometallic nickel catalysts are given in Figures 14 and 15 and in Table 4. The obtained results show that the highest specific surface area had a ZrO₂ support. The incorporation of the NiO phase on the catalyst support

results in decrease in the SSA to 94.4 m²/g for the 5%Ni/ZrO₂ catalyst. A further increase in the Ni content caused a similar effect. The BET results show that the 10%Ni/ZrO₂, 20%Ni/ZrO₂, and 30%Ni/ZrO₂ catalyst exhibited the SSA values equal 85.0, 76.8, and 63.4 m²/g, respectively. The same effect was also observed for the ZrO₂ system promoted by La₂O₃ and CeO₂ oxides. In the case of the ZrO₂ systems promoted by these oxides, a decrease of the specific surface area value was also detected, whereas the catalytic supports 5%CeO₂-ZrO₂ and 5%La₂O₃-ZrO₂ were characterized by the SSA values equal to 98.5 and 92.7, respectively. The same tendency was observed for nickel catalysts supported on the 5%CeO₂-ZrO₂ and 5%La₂O₃-ZrO₂ support material.

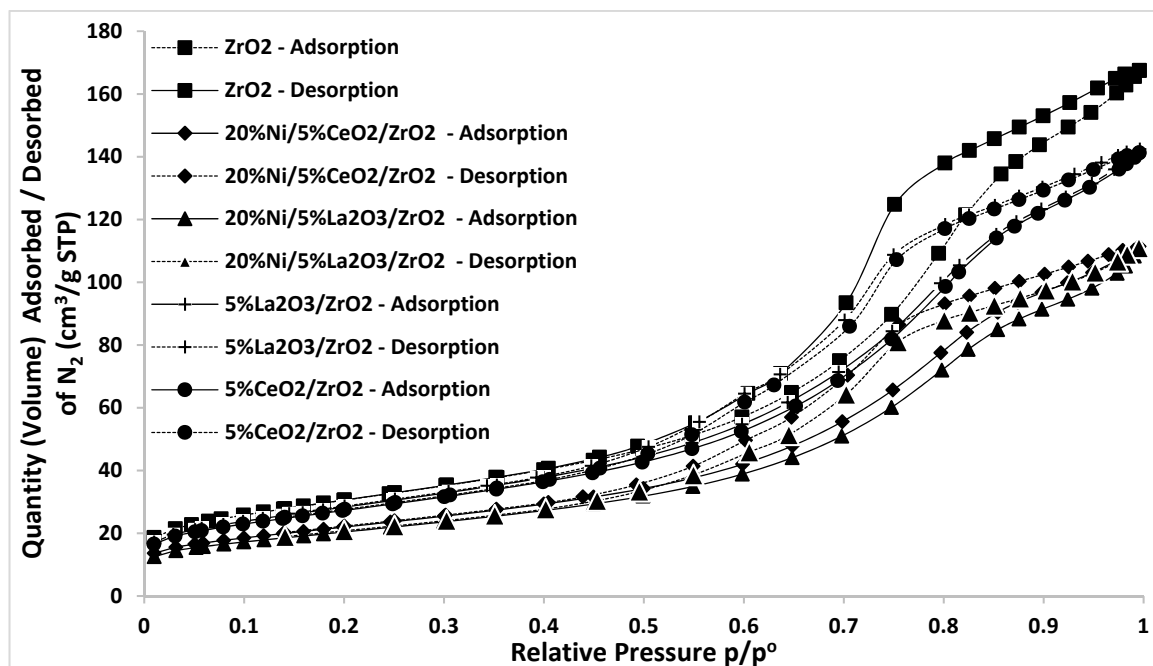


Figure 14. BET adsorption–desorption isotherms for supports and monometallic Ni catalysts calcined in an air atmosphere at 400 °C for 4 h.

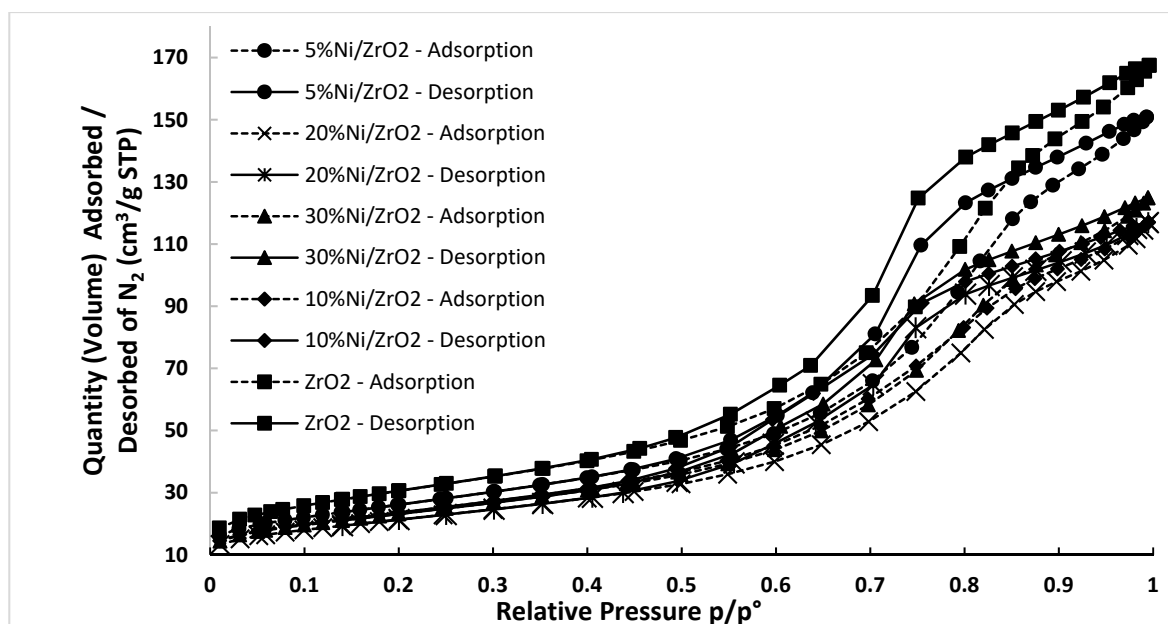


Figure 15. BET adsorption–desorption isotherms for monometallic Ni catalysts calcined in an air atmosphere at 400 °C for 4 h.

The average pore radius values for the investigated catalysts were in the range 2.9–3.4 nm and the monolayer capacity between 0.17 to 0.26 cm³/g values. The highest value (0.26) of monolayer capacity was observed for ZrO₂ oxide, which owned the highest SSA value equal to 109.6 m²/g. All the samples in Figures 14 and 15 show the typical type I isotherm (classification by IUPAC [22]) with a hysteresis loop from $p/p^\circ = 0.45$ due to presence of mesopores. Furthermore, the shapes of hysteresis loops according to IUPAC are H1 type and characteristic for solids consisting of particles crossed by cylindrical channels or made by aggregates (consolidated) or agglomerates (unconsolidated) of spheroidal particles. In both cases, pores can have a uniform size and shape (type H1) [23].

Table 4. Specific surface area and pore size distributions of support and monometallic Ni-supported catalysts calcined in an air atmosphere at 400 °C for 4 h.

Materials	BET Surface Area (m ² /g)	Monolayer Capacity (cm ³ /g)	Average Pore Radius (nm)
ZrO ₂	109.6	0.26	3.4
5%CeO ₂ -ZrO ₂	98.5	0.22	3.2
5%La ₂ O ₃ -ZrO ₂	92.7	0.21	2.9
5%Ni/ZrO ₂	94.4	0.23	3.5
10%Ni/ZrO ₂	85.0	0.18	3.1
20%Ni/ZrO ₂	76.8	0.18	3.4
20%Ni/5%CeO ₂ -ZrO ₂	79.4	0.17	3.2
20%Ni/5%La ₂ O ₃ -ZrO ₂	73.6	0.17	3.4
30%Ni/ZrO ₂	63.4	0.17	3.2

2.5. Acidity of the Catalytic Systems

The acidity properties of support and monometallic Ni catalysts were studied using the TPD-NH₃ technique in order to study their donor-acceptor electron and acid-base properties, and the results are shown in Table 5 and Figures 16–18, respectively. The acidic results clearly show that the lowest total acidity was achieved using the ZrO₂ system (see Figure 16). The introduction of Ni by the impregnation method results in an increase in the acidity in the catalytic systems. These results are explained by the increase in the metallic centers that are present on the catalysts surface and play a crucial role during the adsorption of hydrocarbons in the reforming processes. The results of the acidity show that the addition of the La₂O₃ or CeO₂ oxides into ZrO₂ systems caused a similar effect. The 5%La₂O₃-ZrO₂ and 5%CeO₂-ZrO₂ materials exhibited a higher total acidity compared to the ZrO₂ alone, while 20%Ni catalysts supported on the modified ZrO₂ carrier exhibited lower total acidity compared to the 5%CeO₂-ZrO₂ and 5%La₂O₃-ZrO₂ supports. This result can be explain by the covering of the acidic sites of the supports by metallic oxide particles introduced on the surface. In addition, the introduction of the NiO species during the preparation step may generate interactions between NiO and the support component, which may have an influence on the total acidity of the investigated catalysts. Nickel catalysts 20%Ni/5%La₂O₃-ZrO₂ and 20%Ni/5%CeO₂-ZrO₂, which showed higher total acidity compared to the unpromoted catalytic system exhibited lower catalytic activity in the low temperature range. These results may be explained by the stronger adsorption of hydrocarbon molecules on the metallic surface during the process. In this case, adsorptive methane dissociation of light hydrocarbons or methane to carbon monoxide or carbon dioxide is much more difficult.

Table 5. Amount of NH_3 adsorbed on the surface of ZrO_2 and the reduced monometallic Ni-supported catalysts (reduction for 1 h in pure hydrogen at 500°C) calculated from the surface under the peaks recorded during temperature-programmed desorption measurements.

Catalytic Systems	Total Acidity (mmol/g)	Weak Centers (mmol/g)	Medium Centers (mmol/g)	Strong Centers (mmol/g)
	100–600 $^\circ\text{C}$	100–300 $^\circ\text{C}$	300–450 $^\circ\text{C}$	>450 $^\circ\text{C}$
ZrO_2	0.101	0.054	0.040	0.007
5% CeO_2 - ZrO_2	1.192	0.638	0.470	0.084
5% La_2O_3 - ZrO_2	1.384	0.688	0.608	0.088
5% Ni/ ZrO_2	0.142	0.078	0.060	0.004
10% Ni/ ZrO_2	0.179	0.120	0.540	0.005
20% Ni/ ZrO_2	0.217	0.125	0.086	0.006
20% Ni/5% CeO_2 - ZrO_2	0.620	0.328	0.234	0.057
20% Ni/5% La_2O_3 - ZrO_2	0.734	0.332	0.320	0.081
30% Ni/ ZrO_2	0.360	0.170	0.170	0.020

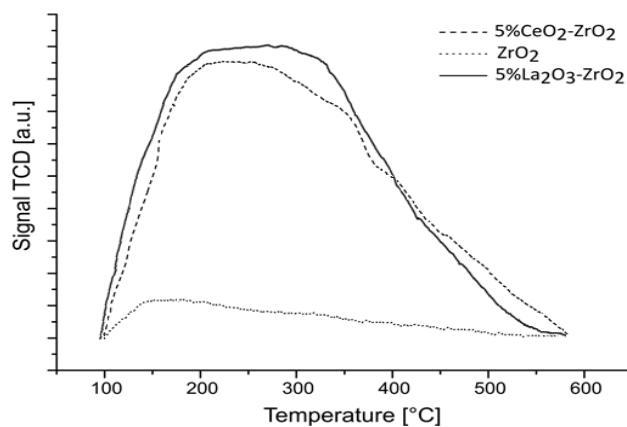


Figure 16. TPD- NH_3 profile of ZrO_2 , 5% CeO_2 - ZrO_2 , and 5% La_2O_3 - ZrO_2 carriers calcined in an air atmosphere for 4 h at 400°C .

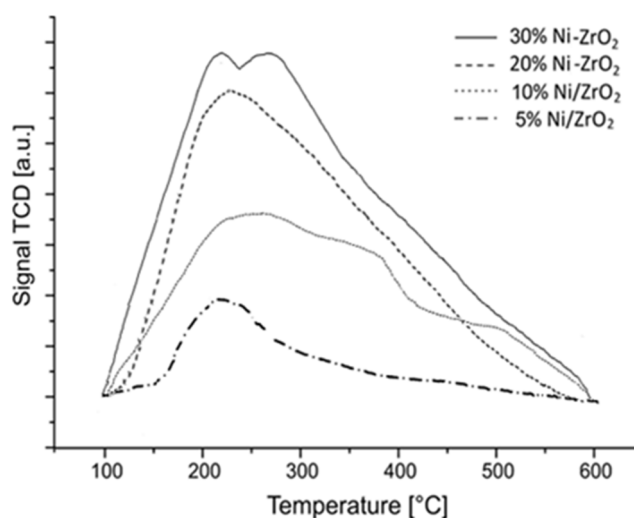


Figure 17. TPD- NH_3 profile of Ni/ ZrO_2 catalysts reduced in hydrogen for 1 h at 500°C .

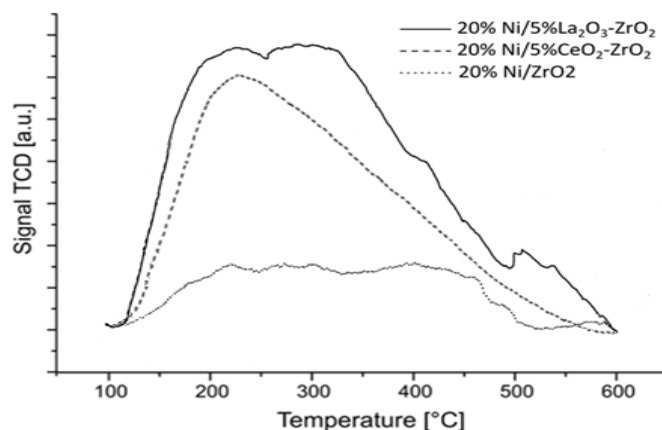


Figure 18. TPD-NH₃ profile of 20%Ni/ZrO₂, 20%Ni/5%CeO₂-ZrO₂, and 20%Ni/5%La₂O₃-ZrO₂ catalysts reduced in hydrogen for 1 h at 500 °C.

2.6. SEM-EDS Measurements of Monometallic Ni Catalysts

SEM-EDS measurements of monometallic nickel catalysts supported on ZrO₂ monoxide carrier were done, and the results are given in Figure 19. The SEM measurements were done to study the surface morphology of the nickel-supported catalysts. The SEM images obtained for various monometallic Ni catalysts with Ni loading in the range 5–20% wt. are shown in Figure 19. The results obtained for the various Ni catalysts show that the Ni catalyst with 10 and 20% wt. of Ni exhibited homogenous distributions of nickel on the catalyst surface, which explains their high activity in the investigated processes. The SEM-EDS measurements performed on the investigated catalysts confirmed the composition of the investigated systems and the absence of impurities derived from the precursor salts used during the preparation of the catalysts.

2.7. Morphology Studies of the Catalytic Material by the ToF-SIMS Technique

The chemical composition of the surface of the spent catalysts was investigated using time-of-flight secondary ion mass spectrometry (ToF-SIMS). The secondary ions Ni⁺, NiOH⁺, Zr⁺, ZrO⁺, ZrOH⁺, and NiZrO⁺ emitted from the surface during the ToF-SIMS experiments were chosen as characteristic for the chemical composition of the catalysts' surface. Their emission intensities are presented in Table 6. Qualitative estimation of Ni surface concentration was made using the relative value of the ratio of Ni⁺ to ZrO⁺ ion emission intensity (Table 7). It can be seen that this ratio, as the function of the nominal nickel content of the catalysts, increases faster for 20% Ni/ZrO₂ and 30%Ni/ZrO₂ catalysts than for the catalyst with a lower nickel content. This observation can be explained by the fact that the dispersion of nickel on the surface of the 20%Ni/ZrO₂ and 30%Ni/ZrO₂ catalysts is higher than for the other catalyst studied.

Table 6. TOF-SIMS results obtained for spent Ni catalysts supported on ZrO₂ oxide.

Ion	Number of Counts × 10 ³			
	5%Ni/ZrO ₂	10%Ni/ZrO ₂	20%Ni/ZrO ₂	30%Ni/ZrO ₂
Ni ⁺	45.0	67.1	180.3	163.9
NiOH ⁺	3.0	5.1	12.0	9.0
Zr ⁺	16.2	17.4	14.5	7.1
ZrO ⁺	56.5	60.3	46.6	18.4
ZrOH ⁺	26.5	29.0	21.6	9.0
NiZrO ⁺	-	0.4	0.5	-

Table 7. The relation between the intensity of selected ions and the nickel content estimated by TOF-SIMS measurements.

Catalyst	Ion Ratio Intensities of Ni ⁺ /ZrO ⁺
5%Ni/ZrO ₂	0.78
10%Ni/ZrO ₂	1.11
20%Ni/ZrO ₂	3.87
30%Ni/ZrO ₂	8.90

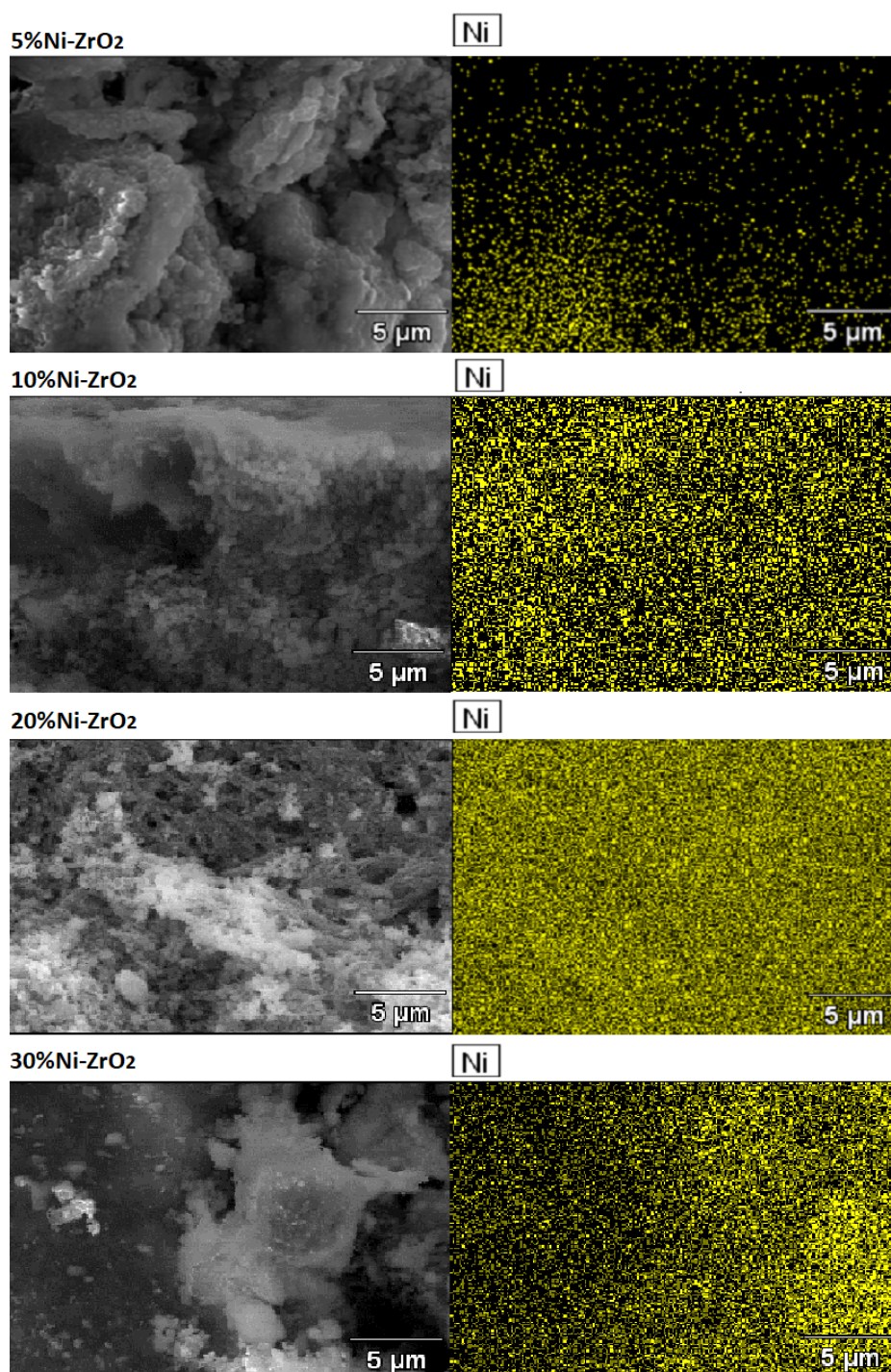


Figure 19. Measurements for monometallic Ni catalysts supported on ZrO₂ oxide calcined at 400 °C in an air atmosphere for 4 h.

An interesting finding concerns the NiZrO^+ ions, which are characteristic for the interaction between Ni species with a catalyst support. The emission of these ions was observed only for the spent 10%Ni/ZrO₂ and 20%Ni/ZrO₂ catalysts. NiZrO^+ ion peak was not observed in TOF-SIMS spectra of the calcined Ni/ZrO₂ catalyst. Therefore, it is reasonable to assume that the high nickel dispersion is not the only factor sufficient to obtain high catalyst activity, but it is also necessary that nickel interacts with the catalyst support to result in the formation of Ni-Zr intermetallic compounds. In summary, the simultaneous presence of high nickel dispersion and nickel support interaction may explain the high activity of the 20%Ni/ZrO₂ catalyst. One can expect that such an interaction will also result in a uniform distribution of the nickel phase on the catalyst support. This prediction is confirmed by the result of the EDS analysis (see Figure 19), which showed the most uniform nickel distribution on the surface of the 20%Ni/ZrO₂ catalyst compared to the rest of the studied systems. In addition, the confirmation of the NiZrO^+ ions emitted from the surface of the nickel-supported catalysts confirms the interaction between NiO and ZrO₂ and explains the calculated reduction degree for the investigated catalysts.

2.8. Thermal Analysis of the Spent Catalysts

The oxy-steam reforming of light hydrocarbons on nickel catalysts involves the risk of coke formation on the catalyst surface, which would lead to its deactivation. Therefore, the resistance to the carbon deposition of the catalysts was investigated in this work. The carbon deposition can be formed during light hydrocarbon decomposition (Equation (1)) or the Boudouard reaction (Equation (2)) [24].



At a higher temperature, the decomposition of hydrocarbons is mostly favorable because this reaction is faster than carbon oxide's decomposition or its reduction [24]. The adsorption of hydrocarbons on the catalyst surface leads to the accumulation of the hydrocarbons on the catalyst surface, causing them to transform into an amorphous carbon at low temperature (below 500 °C). On the other hand, at a high temperature, the main type of carbon is graphite carbon (C_γ) created on the catalyst surface. In this work the carbon deposition was also investigated using a TG-DTA-MS technique. In Figure 20, the MS profiles for $m/z = 44$ (CO₂) obtained during the thermal analysis performed in an air atmosphere using spent Ni catalysts in the temperature range 25–700 °C were presented. As is easily seen, the oxidation of carbon formed on the catalyst surface occurs in three stages for the 20%Ni/ZrO₂ catalyst. The oxidation proceeds up to 700 °C (Figure 20). The peak of CO₂ formation, with the maximum at 130 °C (see MS profile), is really oxidizable of carbon type and may be assigned to the removal of amorphous carbon [25,26]. The second oxidation step (310 °C) is attributed to the oligomerized carbon species, which is signed as β carbon (C_β) or carbides. The last peak situated at about 690 °C is assigned to the oxidation of graphite carbon (C_γ bulk carbides [27,28]). In the case of 20%Ni/5%La₂O₃-ZrO₂, the two peaks of carbon oxidation and for the 20%Ni/5%CeO₂-ZrO₂ catalyst's (Figure 20) three peaks of CO₂ formation on the MS profiles are observed. In all studied cases, the type of carbon deposition with maximum at ca. 290 °C for the catalyst doped by lanthanum oxide and at ca. 310 °C and second peak with maximum 410 °C for the catalyst with cerium oxide addition are related to the removal of amorphous carbon and/or oligomerized carbon, while the third peak with maximum at 690 °C for both catalysts can be assigned to the oxidation of graphite carbon (C_γ or bulk carbides). It is worth mentioning that the main type of carbon deposition in the all cases studied is graphite carbon (C_γ) or bulk carbides. It is also worth mentioning that the addition of CeO₂ into the monometallic Ni/ZrO₂ system reduces the carbon deposit formation on the catalyst surface. This result is very important from the application point of view of these systems on an industrial scale. This result can be explained by the presence of mobile oxygen, which can oxidize the carbon deposit or methane absorbed on the surface of metallic nickel during the investigated processes. This mobile oxygen protects the surface of the catalyst against carbon deposits that can be formed during the process. The

TG-DTA-MS results means that the 20%Ni/ZrO₂ and 20%Ni/5%CeO₂-ZrO₂ catalysts, which exhibited practically similar high activity, also showed high coke resistance, while the least active system in the oxy-steam reforming of LNG (20%Ni/5%La₂O₃-ZrO₂) exhibited the highest amount of carbon deposit formed on its surface (see Figure 20).

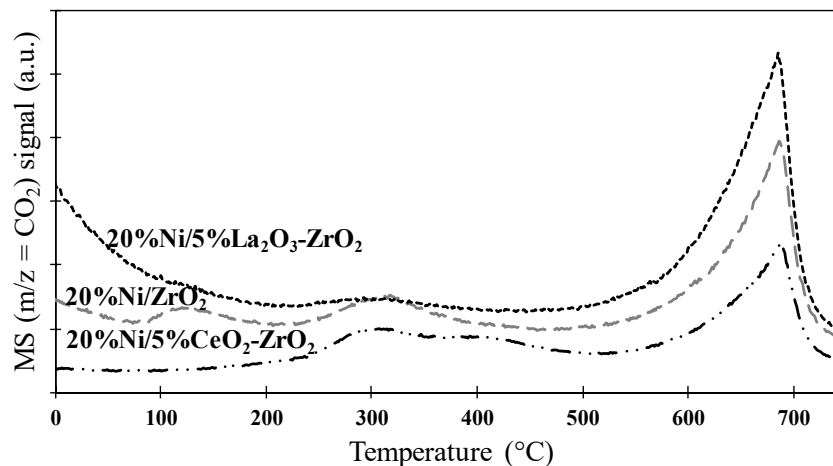


Figure 20. MS profiles for $m/z = 44$ (CO₂) obtained during the thermal analysis performed in an air atmosphere of the spent (after twelve hours of the oxy-steam reforming of LNG process at 700 °C, molar ratio between reagents was used: C:H₂O:O₂ = 1:2.7:0.35, total gas flow 51 cm³/min) monometallic Ni catalysts supported on ZrO₂, 5%CeO₂-ZrO₂, or 5%La₂O₃-ZrO₂ oxides supports.

3. Experimental

3.1. Supports and Catalysts Preparation

ZrO₂ was synthesized by the precipitation method using ammonia as a precipitation agent. The obtained hydroxide of Zr was then filtrated, washed with deionized water, and dried in an air atmosphere at 120 °C for 2h. The ZrO₂ support modified by 5%CeO₂ or 5%La₂O₃ were prepared via impregnation method of previously prepared zirconium oxide. The monometallic nickel catalysts supported on the ZrO₂, 5%CeO₂-ZrO₂, or 5%La₂O₃-ZrO₂ were prepared using the conventional impregnation method. The NiO oxide was introduced on the catalyst surface using Ni(NO₃)₂·6H₂O precursor salt. The support materials were impregnated in 12 h. Then, the catalytic materials were dried for 2h at 80 °C in an air atmosphere and calcined in an air atmosphere for 4h at 400 °C. The Ni content in the catalytic systems were 5, 10, 20, and 30%wt, respectively.

3.2. Characterization of the Catalytic Material

The BET surface area and porosity of the prepared catalytic systems were determined using ASAP 2020 Micrometrics (Surface Area and Porosity Analyzer, Micromeritics Instrument Corporation, Norcross, GA, USA). The morphology of the prepared catalytic systems was studied using a S-4700 scanning electron microscope HITACHI (Tokyo, Japan), equipped with an energy dispersive spectrometer EDS (ThermoNoran, Madison, WI, USA). The reducibility of the Ni catalysts was investigated using an automatic AMI-1 instrument in the temperature range 25–900 °C. In each TPR investigation, about 0.1 g of the sample was used. The acidic properties of the catalytic materials reduced at 500 °C in a mixture of 5%H₂-95%Ar were studied by TPD-NH₃ technique. The phase composition studies of the monometallic nickel-supported catalysts after reduction were carried out using a PANalytical X'Pert Pro MPD diffractometer in Bragg-Brentano reflecting geometry. The carbon deposit formed during the oxy-steam reforming of the CH₄ or LNG process on the catalyst surface was determined using the TG-DTA-MS technique. Thermal analysis was carried out for spent catalytic material on the SETSYS 16/18 thermal analyzer from Setaram (Caluire, France) and quadrupole mass

spectrometer Balzers (Germany). The TG-DTA-MS measurements were performed in the temperature range of 30–1000 °C using a linear temperature rate of 10 °C/min using about 10–20 mg in dynamic conditions gas stream-Air (Air Products). The secondary ion mass spectra for the catalytic materials were recorded using a TOF-SIMS IV mass spectrometer manufactured by Ion-Tof GmbH, Muenster, Germany. The instrument is equipped with a Bi liquid metal ion gun and a high mass resolution time of flight mass analyzer.

3.3. Catalytic Activity Measurements in the Oxy-Steam Reforming of Methane or LNG

The oxy-steam reforming of LNG (a mixture of methane (5%), ethane (0.4%), propane (0.2%), and butane (0.05%)) or methane was performed in a quartz micro-reactor in the temperature range 400–900 °C under atmospheric pressure. Catalytic activity was measured after reaching a stable state of the catalyst system after 30 min of the process. The weight of a catalyst test sample was 0.2 g in all cases. A volumetric ratio between each components of the reaction mixture was as follows: CH₄: H₂O: O₂ = 1:2.7:0.35. Argon was used as a balance gas. In the case of the oxy-steam reforming of LNG, the following molar ratio between reagents was used: C:H₂O:O₂ = 1:2.7:0.35. While the total gas flow rate of the reaction mixture was 51 cm³/min. The analysis of the gaseous reaction mixture composition before and after the reaction was monitored using gas chromatographs equipped with TCD and FID detectors. The catalytic activity results were expressed as CH₄ or higher hydrocarbons conversions were calculated based on the following equation:

$$Con_{C_xH_y} = \left(1 - \frac{(n_{C_xH_y})_{out}}{(n_{C_xH_y})_{in}} \right) \times 100\%$$

The selectivity's to CO or CO₂ were calculated based on the equations presented below:

$$S_{CO} = \frac{(n_{CO})_{out}}{(n_{CO})_{out} + (n_{CO_2})_{out}}$$

$$S_{CO_2} = \frac{(n_{CO_2})_{out}}{(n_{CO})_{out} + (n_{CO_2})_{out}}$$

The hydrogen yield was estimated using the following formula:

$$Y_{H_2} = \left(\frac{\frac{(n_{H_2})_{out}}{2.5}}{\sum (n_{CH_4})_{in} - \sum (n_{CH_4})_{out}} \right) \text{ (in the case of the oxy-steam reforming of methane)}$$

$$Y_{H_2} = \left(\frac{\frac{(n_{H_2})_{out}}{2.73}}{\sum (n_{C_xH_y})_{in} - \sum (n_{C_xH_y})_{out}} \right) \text{ (in the case of the oxy-steam reforming of LNG)}$$

where:

$(n_{C_xH_y})_{out}$ —is the mole fraction of hydrocarbon (methane, ethane, propane and butane) at the reactor entrance;

$(n_{C_xH_y})_{out}$ —is the mole fraction of hydrocarbon (methane, ethane, propane and butane) at the reactor outlet;

$(n_{CO})_{out}$ —is the mole fraction of the CO at the reactor outlet;

$(n_{CO_2})_{out}$ —is the mole fraction of the CO₂ at the reactor outlet;

n_{H_2} —is the mole fraction of the H₂ at the reactor outlet;

$\sum (n_{C_xH_y})_{in}$ —is the sum of the mole fractions of the hydrocarbons at the reactor entrance;

$\sum (n_{C_xH_y})_{out}$ —is the sum of the mole fractions of the hydrocarbons at the reactor outlet.

4. Conclusions

All tested catalysts showed high activity in the temperature range 700–900 °C, but superior activity among of catalytic systems were achieved using 20%Ni/ZrO₂ and 20%Ni/CeO₂-ZrO₂ catalysts. The 20%Ni/ZrO₂ catalyst exhibited above 97% of methane or LNG components conversion at 700 and 100% at 900 °C. The hydrogen yield for this system in the oxy-steam reforming of methane was more than 88% at both temperatures. The results in the oxy-steam reforming of methane reaction also show that the molar ratio between products of H₂ and CO at 700 and 900 °C was equal 2.0 and 2.2 what confirm that produced gas mixture is suitable to generate hydrocarbons via Fischer-Tropsch synthesis. On the other hand, in the case of the oxy-steam reforming of LNG the molar ratio between H₂ and CO was 3.5, 2.0, 1.3 at 600, 700 and 900 °C, while in the oxy-steam reforming of LNG, the hydrogen yield was 58, 74, 57, and 63 at 500, 600, 700, and 900 °C, respectively. It is also worth mentioning that a similar activity in the oxy-steam reforming of the LNG reaction was achieved using 20%Ni/CeO₂-ZrO₂, which also exhibited a high hydrogen yield at 700 °C (60%) and the highest hydrogen production at 900 °C (58%). In addition, this system also showed high stability during the 12-h running time of the reaction. The reduction behavior confirmed the incomplete reduction of NiO in the case of the 20%Ni/CeO₂-ZrO₂ catalyst, which is the result of the solid solution formation and strong interaction between NiO and the support component. In addition, it was also proven that the addition of CeO₂ on the surface of ZrO₂ leads to the creation of a smaller size of crystallites of NiO and metallic nickel on the catalyst surface. TG-DTA-MS measurements performed for the catalytic systems proved that the addition of CeO₂ increases the resistance to carbon deposition, which can be explained by the increased mobility of oxygen that can oxidize the carbon deposit or methane absorbed on the surface of metallic nickel during the investigated processes and thus protects the surface of the catalyst against carbon deposits. In the case of the 20%Ni/5%La₂O₃-ZrO₂ catalyst, the highest carbon deposit was formed on its surface during the process performed during 12 h at 700 °C, which can explain the lowest activity of this systems compared to the rest of the investigated systems. The high activity of the 20%Ni/ZrO₂ catalyst among all of the tested monometallic catalysts is explained by the strong interaction between NiO and ZrO₂, which were confirmed by the TPR measurements and by the detected ToF-SIMS NiZrO⁺ ions created on the catalyst surface for this system.

Author Contributions: The results presented in the work were designed and presented by N.S., M.M., M.N., J.R., J.A., K.C., W.M., M.I.S. and P.M. All authors have read and agreed to the published version of the manuscript.

Funding: The work was funded by the National Science Centre within the “OPUS” Programme, Poland (Grant no. 2018/29/B/ST8/01317).

Conflicts of Interest: The authors declare no conflict of interest.

References

1. Mierczynski, P.; Vasilev, K.; Mierczynska, A.; Maniukiewicz, W.; Szyrkowska, M.I.; Maniecki, T. Bimetallic Au–Cu, Au–Ni catalysts supported on MWCNTs for oxy-steam reforming of methanol. *Appl. Catal. B Environ.* **2016**, *185*, 281–294. [[CrossRef](#)]
2. Mierczynski, P.; Mosinska, M.; Maniukiewicz, W.; Nowosielska, M.; Czyrkowska, A.; Szyrkowska, M.I. Oxy-steam reforming of methanol on copper catalysts. *React. Kinet. Mech. Catal.* **2019**, *127*, 857–874. [[CrossRef](#)]
3. Mierczynski, P. Comparative Studies of Bimetallic Ru–Cu, Rh–Cu, Ag–Cu, Ir–Cu Catalysts Supported on ZnO–Al₂O₃, ZrO₂–Al₂O₃ Systems. *Catal. Lett.* **2016**, *146*, 1825–1837. [[CrossRef](#)]
4. Mierczynski, P.; Vasilev, K.; Mierczynska, A.; Maniukiewicz, W.; Ciesielski, R.; Rogowski, J.; Szyrkowska, M.I.; Trifonov, A.Y.; Dubkov, S.V.; Gromov, D.G.; et al. The effect of gold on modern bimetallic Au–Cu/MWCNT catalysts for the oxy-steam reforming of methanol. *Catal. Sci. Technol.* **2016**, *6*, 4168–4183. [[CrossRef](#)]
5. Mierczynski, P.; Vasilev, K.; Mierczynska, A.; Maniukiewicz, W.; Maniecki, T. Highly selective Pd–Cu/ZnAl₂O₄ catalyst for hydrogen production. *Appl. Catal. A Gen.* **2014**, *479*, 26–34. [[CrossRef](#)]

6. Bang, Y.; Park, S.; Han, S.J.; Yoo, J.; Song, J.H.; Choi, J.H.; Kang, K.H.; Song, I.K. Hydrogen production by steam reforming of liquefied natural gas (LNG) over mesoporous Ni/Al₂O₃ catalyst prepared by an EDTA-assisted impregnation method. *Appl. Catal. B: Environ.* **2016**, *180*, 179–188. [\[CrossRef\]](#)
7. Bang, Y.; Han, S.J.; Yoo, J.; Choi, J.H.; Lee, J.K.; Song, J.H.; Lee, J.; Song, I.K. Hydrogen production by steam reforming of simulated liquefied natural gas (LNG) over nickel catalyst supported on mesoporous phosphorus-modified alumina xerogel. *Appl. Catal. B: Environ.* **2014**, *148*, 269–280. [\[CrossRef\]](#)
8. Park, S.; Yoo, J.; Han, S.J.; Song, J.H.; Lee, E.J.; Song, I.K. Steam reforming of liquefied natural gas (LNG) for hydrogen production over nickel–boron–alumina xerogel catalyst. *Int. J. Hydrogen Energy* **2017**, *42*, 15096–15106. [\[CrossRef\]](#)
9. Gil Seo, J.; Youn, M.H.; Park, S.; Chung, J.S.; Song, I.K. Hydrogen production by steam reforming of liquefied natural gas (LNG) over Ni/Al₂O₃–ZrO₂ xerogel catalysts: Effect of calcination temperature of Al₂O₃–ZrO₂ xerogel supports. *Int. J. Hydrogen Energy* **2009**, *34*, 3755–3763.
10. Li, K.; Chang, X.; Pei, C.; Li, X.; Chen, S.; Zhang, X.; Assabumrungrat, S.; Zhao, Z.-J.; Zeng, L.; Gong, J. Ordered mesoporous Ni/La₂O₃ catalysts with interfacial synergism towards CO₂ activation in dry reforming of methane. *Appl. Catal. B: Environ.* **2019**, *259*, 118092. [\[CrossRef\]](#)
11. Maniecki, T.; Stadnichenko, A.I.; Maniukiewicz, W.; Bawolak, K.; Mierczynski, P.; Boronin, A.I.; Jozwiak, W.K. An active phase transformation on surface of Ni–Au/Al₂O₃ catalyst during partial oxidation of methane to synthesis gas. *Kinet. Catal.* **2010**, *51*, 573–578. [\[CrossRef\]](#)
12. Dantas, S.C.; Escritori, J.C.; Soares, R.R.; Hori, C.E. Effect of different promoters on Ni/CeZrO₂ catalyst for autothermal reforming and partial oxidation of methane. *Chem. Eng. J.* **2010**, *156*, 380–387. [\[CrossRef\]](#)
13. Wu, H.; Pantaleo, G.; La Parola, V.; Venezia, A.M.; Collard, X.; Aprile, C.; Liotta, L.; Liotta, L. Bi- and trimetallic Ni catalysts over Al₂O₃ and Al₂O₃–MO_x (M=Ce or Mg) oxides for methane dry reforming: Au and Pt additive effects. *Appl. Catal. B: Environ.* **2014**, *156*, 350–361. [\[CrossRef\]](#)
14. Takeguchi, T.; Furukawa, S.-N.; Inoue, M.; Eguchi, K. Autothermal reforming of methane over Ni catalysts supported over CaO–CeO₂–ZrO₂ solid solution. *Appl. Catal. A: Gen.* **2003**, *240*, 223–233. [\[CrossRef\]](#)
15. Bachiller-Baeza, B.; Mateos-Pedrero, C.; Soria, M.A.; Guerrero-Ruiz, A.; Rodemerck, U.; Rodríguez-Ramos, I. Transient studies of low-temperature dry reforming of methane over Ni–CaO/ZrO₂–La₂O₃. *Appl. Catal. B: Environ.* **2013**, *129*, 450–459. [\[CrossRef\]](#)
16. Pantaleo, G.; La Parola, V.; Deganello, A.F.; Calatozzo, P.; Bal, R.; Venezia, A.M. Synthesis and support composition effects on CH₄ partial oxidation over Ni–CeLa oxides. *Appl. Catal. B: Environ.* **2015**, *164*, 135–143. [\[CrossRef\]](#)
17. Галахов, С.И.; Sidorova, O.I. Effect of a precursor on the phase composition and particle size of the active component of Ni–ZrO₂ catalytic systems for the oxidation of methane into syngas. *Russ. J. Phys. Chem. A* **2014**, *88*, 1629–1636. [\[CrossRef\]](#)
18. Hoang, D.L.; Lieske, H. Effect of hydrogen treatments on ZrO₂ and Pt/ZrO₂ catalysts. *Catal. Lett.* **1994**, *27*, 33–42. [\[CrossRef\]](#)
19. Rhodes, M.D.; Pokrovski, K.A.; Bell, A.T. The effects of zirconia morphology on methanol synthesis from CO and H₂ over Cu/ZrO₂ catalysts Part II. Transient-response infrared studies. *J. Catal.* **2005**, *233*, 210–220. [\[CrossRef\]](#)
20. Jia, X.; Zhang, X.; Rui, N.; Hu, X.; Liu, C.-J. Structural effect of Ni/ZrO₂ catalyst on CO₂ methanation with enhanced activity. *Appl. Catal. B: Environ.* **2019**, *244*, 159–169. [\[CrossRef\]](#)
21. Nichele, V.; Signoretto, M.; Pinna, F.; Menegazzo, F.; Rossetti, I.; Cruciani, G.; Cerrato, G.; Di Michele, A. Ni/ZrO₂ catalysts in ethanol steam reforming: Inhibition of coke formation by CaO-doping. *Appl. Catal. B: Environ.* **2014**, *150*, 12–20. [\[CrossRef\]](#)
22. Cranston, R.; Inkley, F. 17 The Determination of Pore Structures from Nitrogen Adsorption Isotherms. *Advances in Catalysis* **1957**, *9*, 143–154.
23. Leofanti, G.; Padovan, M.; Tozzola, G.; Venturelli, B. Surface area and pore texture of catalysts. *Catal. Today* **1998**, *41*, 207–219. [\[CrossRef\]](#)
24. Roh, H.-S.; Jun, K.-W. Carbon Dioxide Reforming of Methane over Ni Catalysts Supported on Al₂O₃ Modified with La₂O₃, MgO, and CaO. *Catal. Surv. Asia* **2008**, *12*, 239–252. [\[CrossRef\]](#)
25. Herrera, J.E.; Resasco, D.E. In situ TPO/Raman to characterize single-walled carbon nanotubes. *Chem. Phys. Lett.* **2003**, *376*, 302–309. [\[CrossRef\]](#)

26. Chen, J.; Yang, X.; Li, Y. Investigation on the structure and the oxidation activity of the solid carbon produced from catalytic decomposition of methane. *Fuel* **2010**, *89*, 943–948. [[CrossRef](#)]
27. Tsyganok, A. Dry reforming of methane over catalysts derived from nickel-containing Mg–Al layered double hydroxides. *J. Catal.* **2003**, *213*, 191–203. [[CrossRef](#)]
28. Bradford, M.C.; Vannice, M.A. Catalytic reforming of methane with carbon dioxide over nickel catalysts I. Catalyst characterization and activity. *Appl. Catal. A: Gen.* **1996**, *142*, 73–96. [[CrossRef](#)]



© 2020 by the authors. Licensee MDPI, Basel, Switzerland. This article is an open access article distributed under the terms and conditions of the Creative Commons Attribution (CC BY) license (<http://creativecommons.org/licenses/by/4.0/>).